Smoothed Finite Element Method

K.Y. DAI [1] and G.R. LIU [1, 2]

[1] Singapore-MIT Alliance (SMA), E4-04-10, 4 Engineering Drive 3, Singapore, 117576

[2] Center for Advanced Computations in Engineering Science (ACES), Department of Mechanical Engineering, National University of Singapore, 10 Kent Ridge Crescent, Singapore, 119260

Abstract—In this paper, the smoothed finite element method (SFEM) is proposed for 2D elastic problems by incorporation of the cell-wise strain smoothing operation into the conventional finite elements. When a constant smoothing function is chosen, area integration becomes line integration along cell boundaries and no derivative of shape functions is needed in computing the field gradients. Both static and dynamic numerical examples are analyzed in the paper. Compared with the conventional FEM, the SFEM achieves more accurate results and generally higher convergence rate in energy without increasing computational cost. In addition, as no mapping or coordinate transformation is performed in the SFEM, the element is allowed to be of arbitrary shape. Hence the well-known issue of the shape distortion of isoparametric elements can be resolved.

Index Terms —finite element method (FEM), Gauss quadrature, isoparametric element, smoothed finite element method (SFEM), strain smoothing.

I. INTRODUCTION

After more than half a century of development, finite element method (FEM) has become a very powerful technique for numerical simulations in engineering and science. Mapped elements, such as the well-known isoparametric elements, play a very important role in FEM. When using a mapped element, a basic requirement is that the element has to be convex and a violent distortion is not permitted so that a one-to-one coordinate correspondence between the physical and natural coordinates associated with an element can be guaranteed. In numerical implementation, the determinant of the Jacobian matrix should be always checked for its positivity to avoid severely distorted elements [1, 2].

Recently, a stabilized conforming nodal integration has been proposed using a strain smoothing technique for a Galerkin mesh-free method which shows higher efficiency, desired accuracy and convergent properties [3]. In addition, a linear exactness can be guaranteed in the solution of Galerkin weak-form based mesh-free methods. In this paper, we implement the strain projection idea to formulate and code a novel method, smoothed finite element method (SFEM) [4, 5], which combines the existing FEM technology with the strain smoothing technique. We will demonstrate through intensive case studies the significant

benefits arising from this novel combination.

II. STRIAN SMOOTHING

A 2D static elasticity problem can be described by equilibrium equation in the domain Ω bounded by Γ

$$\sigma_{ij,j} + b_i = 0 \quad \text{in } \Omega \tag{1}$$

which subject to the boundary conditions: $\sigma_{ij} n_j = t_i$ on Γ_t and $u_i = \bar{u}_i$ on Γ_u, where σ_{ij} is the component of stress tensor and b_i the component of body force; n_i is the unit outward normal. Its variational weak form is derived as

$$\int_{\Omega} \delta \nabla_s(u)_{ij} D_{ijkl} \nabla_s(u)_{kl} d\Omega - \int_{\Gamma_t} \delta u_i t_i d\Gamma = 0 \tag{2}$$

In the SFEM, elements are used as in the FEM. Galerkin weak form given in Eq. (2) is applied and integration is performed on the basis of element. Depending on the requirement of stability, an element may be further subdivided into several smoothing cells (SC) [4]. A smoothing operation is performed for each smoothing cell within an element, as expressed by

$$\nabla u^h(\mathbf{x}_C) = \int_{\Omega_C} \nabla u^h(\mathbf{x}) \Phi(\mathbf{x} - \mathbf{x}_C) d\Omega \tag{3}$$

where Φ is a smoothing function. For simplicity, a piecewise constant function is applied here, as given by $\Phi(\mathbf{x} - \mathbf{x}_C) = 1/A_C$ ($\mathbf{x} \in \Omega_C$) and $\Phi(\mathbf{x} - \mathbf{x}_C) = 0$ ($\mathbf{x} \notin \Omega_C$), where the area of the cell $A_C = \int_{\Omega_C} d\Omega$ and Ω_C is the domain occupied by the smoothing cell (see Fig. 1). Substituting Φ into Eq. (3), one can get the smoothed gradient of displacement

$$\widetilde{\nabla} u^h(\mathbf{x}_C) = \int_{\Gamma_C} u^h(\mathbf{x}) \mathbf{n}(\mathbf{x}) \Phi(\mathbf{x} - \mathbf{x}_C) d\Gamma$$
$$= \frac{1}{A_C} \int_{\Gamma_C} u^h(\mathbf{x}) \mathbf{n}(\mathbf{x}) d\Gamma \tag{4}$$

The displacement field in an element can be approximated as in the FEM by

$$\mathbf{u}^h(\mathbf{x}) = \sum_{NP} N_I \mathbf{u}_I \tag{5}$$

Similarly the smoothed strain in discrete form can be obtained as follows

$$\widetilde{\boldsymbol{\varepsilon}}^h(\mathbf{x}_C) = \sum_{NP} \widetilde{\mathbf{B}}_I(\mathbf{x}_C)\mathbf{d}_I \tag{6}$$

where $\widetilde{\mathbf{B}}_I$ is the smoothed strain matrix. For a 2D case

$$\widetilde{\mathbf{B}}_I(\mathbf{x}_C) = \begin{bmatrix} \widetilde{b}_{I1}(\mathbf{x}_C) & 0 \\ 0 & \widetilde{b}_{I2}(\mathbf{x}_C) \\ \widetilde{b}_{I2}(\mathbf{x}_C) & \widetilde{b}_{I1}(\mathbf{x}_C) \end{bmatrix}$$

where $\widetilde{b}_{Ik}(\mathbf{x}_C) = \dfrac{1}{A_C}\displaystyle\int_{\Gamma_c} N_I(\mathbf{x})n_k(\mathbf{x})d\Gamma, \ (k=1,2)$. The smoothed element stiffness matrix can be obtained by assembly of all the smoothing cells associated with the element, i.e.,

$$\mathbf{K}_e = \sum_C \widetilde{\mathbf{B}}_C^T \mathbf{D} \widetilde{\mathbf{B}}_C \tag{7}$$
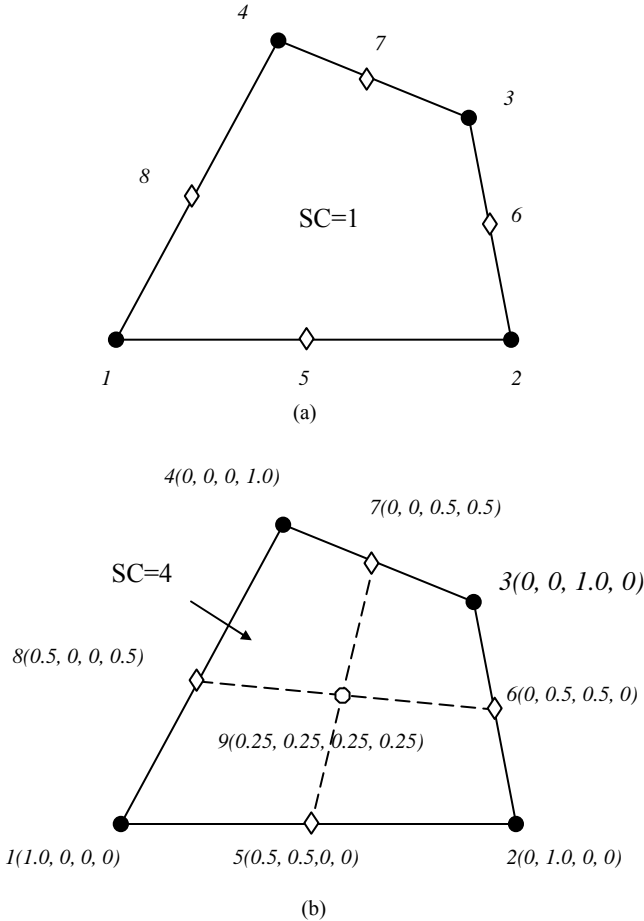

(a)

(b)

Fig 1. Division of SC and Construction of shape functions

III. SFEM SHAPE FUNCTIONS AND STABILITY CONDITION

In the SFEM, as only the shape function itself is involved in calculating the gradient matrix, very simple shape functions can be utilized at Gauss points on the edges of a cell. The SFEM shape functions should possess the following criteria: (1) Delta function: $N_i(\mathbf{x}_j) = \delta_{ij}$; (2) Partition of unity: $\sum_{i=1}^{n} N_i(\mathbf{x}) = 1$; (3) Linear compatibility: $\sum_{i=1}^{n} N_i(\mathbf{x})\mathbf{x}_i = \mathbf{x}$; (4) $N_i(\mathbf{x}) \geq 0$. Any shape functions satisfying the four conditions can be used in the SFEM.

Let's take a quadrilateral element for example. For any point on its side, e.g., the midpoints #5, #6, #7 and #8 shown in Fig. 1(b), the values of the shape functions are calculated linearly using shape functions of two related nodes on the side. The values of the shape functions at point #9, the intersection of two bimedians, are the average of those at the four midpoints. If this point happens to coincide with one field node, its shape functions should adopt the values of this node accordingly. Shape functions for other interior points needed in line integrations can be easily obtained in a similar way [4].

In eigenvalue analysis of a free element using SFEM, if an entire element is used as one smoothing cell (SC=1) as shown in Fig. 1(a), five spurious zero-energy modes are found, which is similar to the case of FEM using one Gauss point. Later on it is found that one SC is equivalent to three independent relations ($n_\sigma = 3$). The difference between the displacement freedoms n_u and the constraints is the number of spurious modes, and thus $n_u - n_\sigma = 5$. The one cell smoothed integration cannot suppress the well-know hourglass modes. This means that the use of smoothed integration can still give rise to instabilities. Then we subdivide the element into four cells (SC=4) and now $n_u - n_\sigma < 0$. Comparing the results with those of FEM using 2×2 quadrature, Once again the modes of the two methods coincide with each other. It is also found that, except three rigid-body-movement modes, no zero-energy modes exist in them, which demonstrates the stable integration. Therefore, SC=4 is recommended in 4-node SFEM in this paper.

Further study of more general polygonal elements, we can conclude that to ensure stiffness stability, the number of constraints arising from SC should not be less than that of the free displacement freedoms [6], i.e, $n_u \leq n_\sigma$. A dodecagonal element is investigated to verify this point. The element is divided into 2, 4, 6 and 12 cells. For the first three the rank of the stiffness matrix is the same as n_σ, which is smaller than the n_u and accordingly standard patch test fails. For the last case (SC=12), the patch test is well passed.

(8)

IV. DYNAMIC ANALYSIS

When inertia and damping effects are considered, the discrete governing equations can be obtained as in FEM [7]

$$\mathbf{M}\ddot{\mathbf{d}} + \mathbf{C}\dot{\mathbf{d}} + \mathbf{f}^{\text{int}} = \mathbf{f}^{ext} \tag{8}$$

where $\mathbf{d}$ is the vector of general nodal displacements and

$$\mathbf{f}^{ext} = \int_{\Omega} \mathbf{N}^T \mathbf{b} d\Omega + \int_{\Gamma_t} \mathbf{N}^T \mathbf{t} d\Gamma \qquad (9)$$

$$\mathbf{M} = \int_{\Omega} \mathbf{N}^T \boldsymbol{\rho} \mathbf{N} d\Omega \qquad (10)$$

$$\mathbf{C} = \int_{\Omega} \mathbf{N}^T \mathbf{c} \mathbf{N} d\Omega \qquad (11)$$

Now in SFEM the internal nodal force is expressed as

$$\mathbf{f}_C^{int} = \int_{\Omega_C} \widetilde{\mathbf{B}}^T \widetilde{\boldsymbol{\sigma}} d\Omega \qquad (12)$$

If no damping or forcing terms exists in Eq. (8), after introducing the smoothed versions of strain and stress, for linear problems it reduces to

$$\mathbf{M}\ddot{\mathbf{d}} + \widetilde{\mathbf{K}}\mathbf{d} = \mathbf{0} \qquad (13)$$

where the smoothed stiffness matrix is given as

$$\widetilde{\mathbf{K}}_{IJ} = \sum_C \int_{\Omega_C} \widetilde{\mathbf{B}}_I^T \mathbf{D} \widetilde{\mathbf{B}}_J d\Omega \qquad (14)$$

A general solution of such an equation can be written as $\mathbf{d} = \overline{\mathbf{d}} \exp(i\omega t)$. Then on its substitution into Eq. (13), the frequency ω can be found from

$$(-\omega^2 \mathbf{M} + \widetilde{\mathbf{K}})\overline{\mathbf{d}} = \mathbf{0} \qquad (15)$$

Total Lagrange formulation is used when geometrical nonlinear behavior is considered. The initial position of a material point in a body is given by $\mathbf{X}$ in a fixed reference configuration and the total displacement at time t_n is denoted as $\mathbf{u}_n$ then the current deformed configuration is described by

$$\mathbf{x}_n = \mathbf{X} + \mathbf{u}_n \qquad (16)$$

The current deformation is measured by the deformation gradient matrix relative to $\mathbf{X}$ given by

$$\mathbf{F}_n = \frac{\partial \mathbf{x}_n}{\partial \mathbf{X}} \qquad (17)$$

In a similar way as used for strain, deformation gradient in Eq. (17) needs to be smoothed in SFEM as

$$\widetilde{F}_{ij}(\mathbf{X}_C) = \frac{1}{A_C^X} \int_{\Omega_C^X} \left[\frac{\partial u_i^h}{\partial X_j} + \delta_{ij} \right] d\Omega = \frac{1}{A_C^X} \int_{\Omega_C^X} \left[\frac{\partial u_i^h}{\partial X_j} \right] d\Omega + \delta_{ij}$$

$$= \frac{1}{A_C^X} \int_{\Gamma_C^x} (u_i^h N_j) d\Gamma + \delta_{ij} = \widetilde{e}_{ij}(\mathbf{X}_C) + \delta_{ij} \qquad (18)$$

where $A_C^X = \int_{\Omega_L^X} d\Omega$ is the initial area of the smoothing cell in study and

$$\widetilde{e}_{ij}(\mathbf{X}_C) = \frac{1}{A_C^X} \int_{\Gamma_C^x} (u_i^h n_j) d\Gamma, \text{ or } \widetilde{e}_{ij}(\mathbf{X}_C) = \sum_I \widetilde{b}_{jI}^C d_{iI} \qquad (19)$$

where $\widetilde{b}_{jI}^C = \frac{1}{A_C^X} \int_{\Gamma_C^x} (N_I n_j) d\Gamma$.

V. NUMERICAL EXAMPLES

A. Standard Patch Test

In the standard patch test, linear displacements are imposed along the boundaries of a square patch with at least one interior node. Satisfaction of the patch test requires that the displacements of all the interior nodes follow "exactly" (to machine precision) the same function of the prescribed displacements. Two types of discretization are used, as shown in Fig. 2: one with 10×10 regular elements and the other with irregular interior nodes. It is found that the SFEM can pass the patch test within machine precision regardless of the number of SC used and the shape of elements.
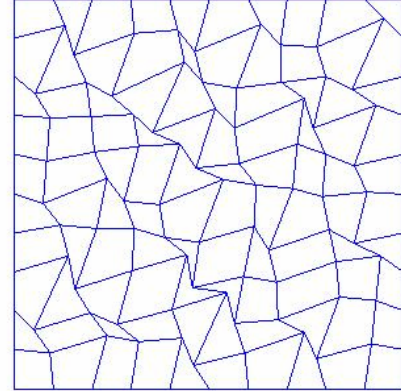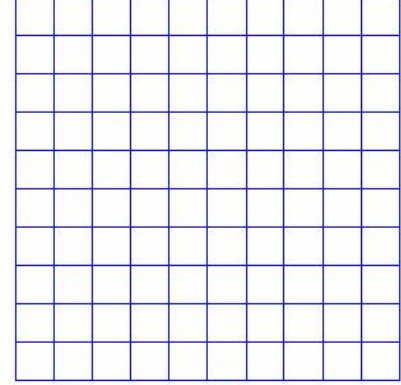

Fig. 2. Meshes for standard patch test.

B. Infinite Plate with a Circular Hole

A plate with a central circular hole (as shown in Fig. 3) is investigated that subjected to a unidirectional tensile load of 1.0 N/m at infinity in the x-direction [8]. Plane strain condition is considered and E=$1.0 \times 10^3 N/m^2$, $v = 0.3$. Each element is divided into four smoothing cells. The computed displacement and stress are selectively demonstrated in Fig. 4 and compared with the exact solutions. When calculating the energy three schemes are adopted. In S44, SC/GP=4 is used for calculation of both displacement and stress (or energy). Likewise in S11, SC/GP=1 is employed all the time. Instead in S41, SC/GP=4 is used only for displacement while reduced integration SC/GP=1 is used for post-processing of stress and energy. From our results it is observed that the

computed displacements and stresses are in good agreement with the analytical solutions. The convergence rates in displacement and energy are demonstrated in Fig. 5. It is observed that a comparable convergence speeds in displacement and energy have been obtained but those of SFEM are once again more accurate than of FEM.
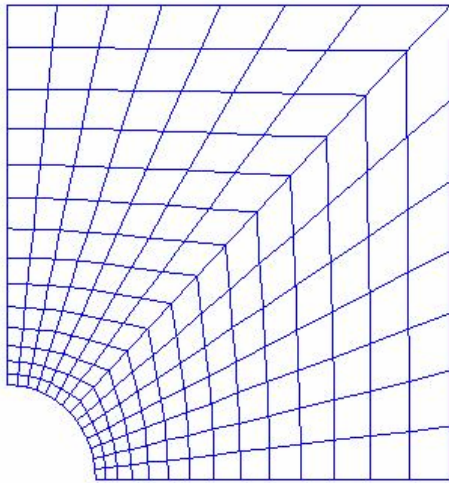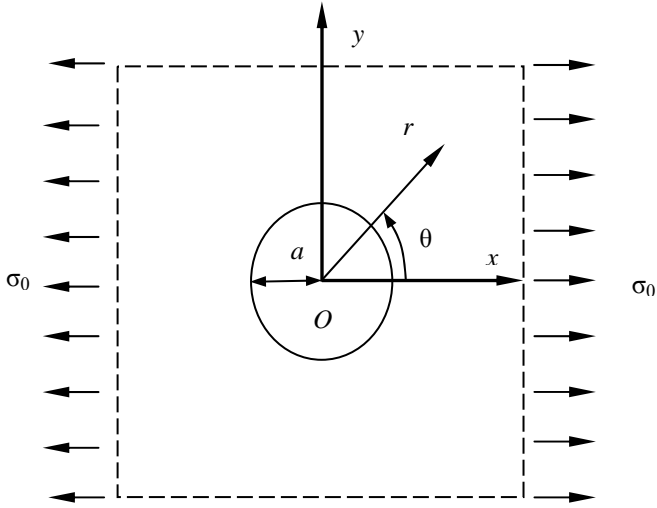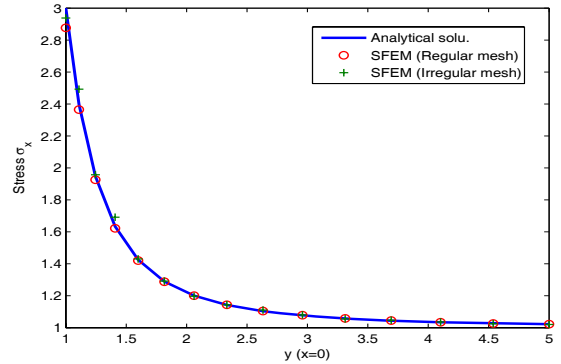

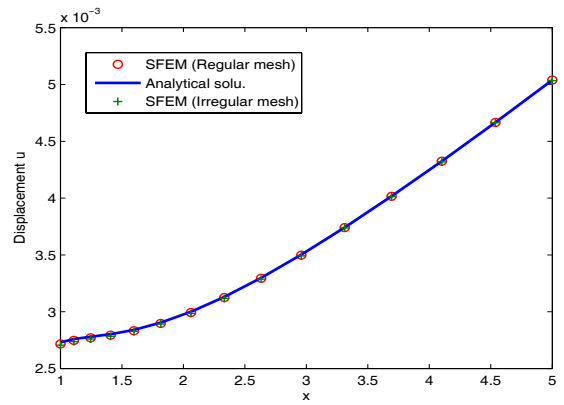Fig. 3. Infinite plate with a circular hole and its meshes.

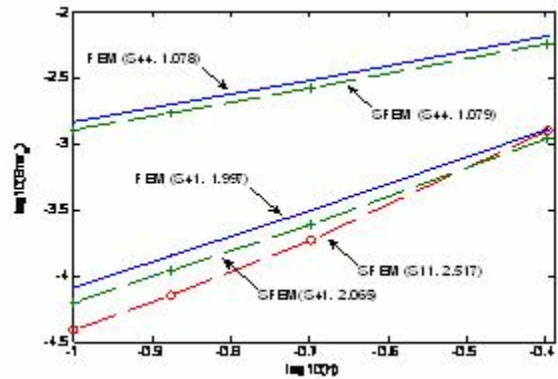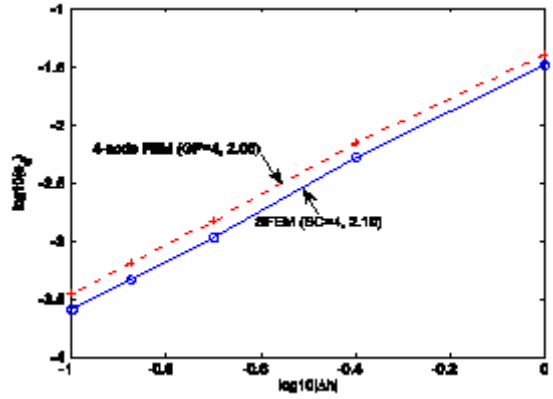Fig. 4. The exact and computed displacements and stresses.

Fig. 5. The convergence rates in displacement and energy.

C. Free Vibration Analysis of a Variable Cross-Section Beam

A cantilever beam with variable cross-section is examined as shown in Fig. 6. The following parameters are used: L=10; $H(0)$=5, $H(L)$=3, t=1.0, $E = 3.0 \times 10^7$, v=0.3, and ρ =1.0. The first four natural frequencies are computed using FEM/SFEM as given in Table I. It can be observed that the SFEM gives better results than FEM when using the same mesh.
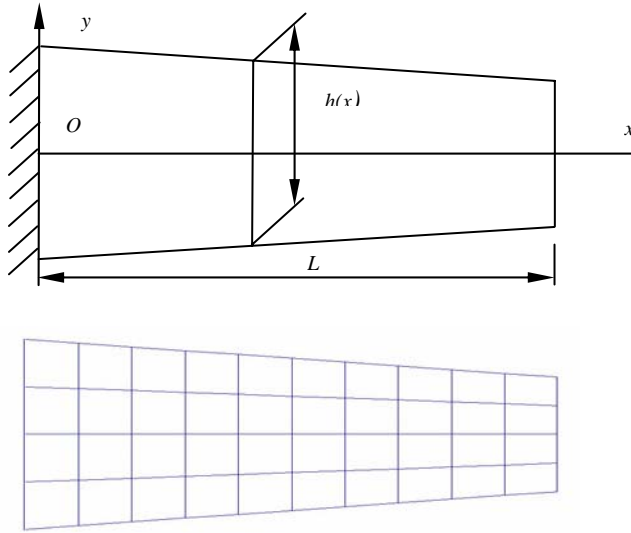

Fig. 6. A cantilever beam with variable cross-section and its meshes.

TABLE I
First four natural frequencies ($\times 10^3$ rad/s) of a variable cross-section cantilever beam using FEM/SFEM

No. of elements	No. of nodes	SFEM	FEM (4-node)	FEM (8-node)
10×4	55 (4-node ele.) 149 (8-nodes ele.)	0.26114 0.91563 0.95127 1.82958	0.26514 0.94891 0.95401 1.95759	0.26177 0.91881 0.95219 1.85568
20×10	231 (4-node ele.) 661 (8-nodes ele.)	0.26166 0.91758 0.95184 1.84773	0.26246 0.92490 0.95251 1.87744	0.26162 0.91783 0.95201 1.85261
40×20	861 (4-node ele.)	0.26160 0.91767 0.95193 1.85118	0.26181 0.91952 0.95211 1.85867	

D. Explicit forced vibration of a spherical shell

To clearly demonstrate the effect of geometrical nonlinearity if compared with the linear elastic analysis, we use the following material properties as well as the geometric parameters of the spherical shell in this example: $R = 12.1$ cm in, $t = 0.04$ cm, $\phi = 10.9°$, $P = 445$ N, $E = 68.9$ GPa, $v = 0.3$. $\rho = 2.82 \times 10^3 \text{kg/m}^3$. A central difference procedure is used to integrate the kinematics explicitly through time. As the method is conditionally stable a very small time step is permitted that solely depends on the computational model. In this example, $\Delta t = 10^{-8}$ sec is used. Fig. 7(a) shows the comparison of dynamic responses between linear and nonlinear elastic solutions. It is observed that both the period and amplitude of nonlinear response are about two times of those of linear case. In Fig. 7(b) dynamic relaxation is introduced with $\alpha = 10^4$ and $\beta = 0$. We notice that the response is damping out gradually and static deflection can be approximately retrieved. The static linear deflection is located roughly at the middle part of the curves whereas the static nonlinear deflection is very close to the peak amplitude, which is agreeable with those using static nonlinear analysis of Newton-Raphson procedure [9].
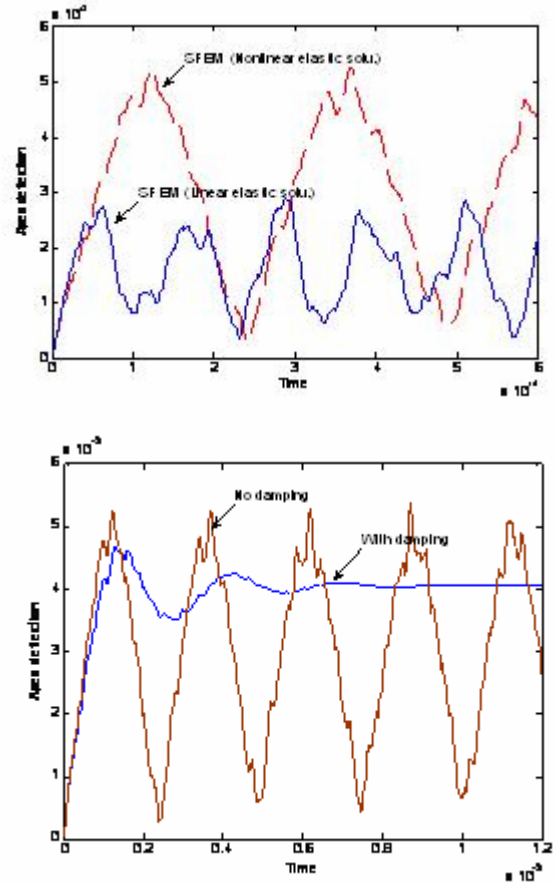

Fig. 7. Linear and nonlinear elastic dynamic responses of a spherical shell under concentrated loading.

VI. Conclusion

In this work, the smoothed finite element method (SFEM) is presented based on the framework of FEM by incorporating a strain-smoothing technique. In SFEM, field gradients are computed directly only using shape functions itself. As no coordinate transformation or mapping is performed in SFEM, restriction placed on the shape of elements in FEM can be removed. Its convergence rates in both displacement and energy of SFEM are comparable as compared with its counterpart of 4-node isoparametric finite elements but the numerical results of SFEM are generally more accurate than FEM solutions. The conclusion is also verified by the free vibration analysis. The energy rate obtained using S41 is two times higher as compared with that using S44. Numerical experiments also show that the SFEM is generally more efficient than FEM especially for a mesh divided with very large number of elements.

References

[1] O. C. Zienkiewicz and R. L. Taylor, *The finite element method (Fifth edition)*. Oxford: Butterworth Heinemann, 2000.

[2] G. R. Liu and S. S. Quek, *The finite element method: a practical course*. Oxford: Butterworth Heinemann, 2003.

[3] J. S. Chen, C. T. Wu, S. Yoon and Y. You, "A stabilized conforming nodal integration for Galerkin meshfree method", *Int. J. Numer. Meth. Engng.,*; vol. 50. pp. 435-466, 2001.

[4] G. R. Liu, K. Y. Dai, T. T. Nguyen, "A smoothed finite element method for mechanics problems", *Comput. Mech.*, (in press, appear online), 2006.

[5] G. R. Liu, T. T. Nguyen, K. Y. Dai and K. Y. Lam, "Theoretical aspects of the smoothed finite element method (SFEM)", *Int. J. Numer. Method Engng.* (in press), 2006.

[6] K. Y. Dai, G. R. Liu and X. Han, "An n-sided polygonal smoothed finite element method (nSFEM) for solid mechanics", *Finite Elements Anal. Design* (Revised), 2006.

[7] K. Y. Dai and G. R. Liu, "Free and forced vibration analysis using the smoothed finite element method (SFEM)", *J. Sound Vib.* (in press), 2006.

[8] S. P. Timoshenko, J. N. Goodier, *Theory of Elasticity*, 3rd Edition. New York: McGraw-Hill, 1970.

[9] K. Kleiber and C. Wozniak, *Nonlinear Mechanics of Structures*, Dordrecht: Kluwer Academic Publishers, 1991.